Optical diffraction of second-harmonic signals in the $LiBO_2$-Nb_2O_5 glasses induced by self-organized $LiNbO_3$ crystallites

B. Harihara Venkataraman, N. Syam Prasad, and K. B. R. Varma[a)]
Materials Research Centre, Indian Institute of Science, Bangalore, India

Vincent Rodriguez
Laboratoire de Physico—Chimie Moleculaire, UMR 5803 CNRS—Universite, Bordeaux, France

Mario Maglione, R. Vondermuhll, and J. Etourneau
Institute for Condensed Matter Chemistry of Bordeaux (ICMCB)—Universite, Bordeaux 1, France

The nanocrystallites (≈3 nm) of $LiNbO_3$, evolved in the $(100-x)LiBO_2$-xNb_2O_5 ($5 \leqslant x \leqslant 20$, in molar ratio) glass system exhibited intense second-harmonic signals in transmission mode when exposed to infrared (IR) light at $\lambda = 1064$ nm. The second-harmonic waves were found to undergo optical diffraction which was attributed to the presence of self-organized submicrometer-sized $LiNbO_3$ crystallites that were grown within the glass matrix along the parallel damage fringes created by the IR laser radiation. Micro-Raman studies carried out on the laser-irradiated samples confirmed the self-organized crystallites to be $LiNbO_3$.

Glass–ceramics comprising well-known ferroelectric crystalline phases ($BaTiO_3$, $PbTiO_3$, $LiNbO_3$, $LiTaO_3$, $SrBi_2Ta_2O_9$, etc.) have been investigated from their dielectric, pyroelectric, ferroelectric, electro, and nonlinear optical applications viewpoint.[1–6] Among important ferroelectric materials that were crystallized either from their corresponding glassy phases or grown in an optically compatible host glass matrices, lithium niobate ($LiNbO_3$) has attracted the attention of many glass researchers around the globe, because of its promising electro-optic and nonlinear optic properties that are exploited in the fabrication of optical waveguides, modulators, and switches.[7–12]

In most of the studies that were reported to date, either the constituent oxides or the prereacted $LiNbO_3$ was melted along with optically compatible host glass matrix and $LiNbO_3$ crystallites were grown within matrix. In this paper, we report an alternate and economically more viable route of obtaining nanocrystals of $LiNbO_3$ in $LiBO_2$ glass matrix as a result of the *in situ* chemical reaction. The results concerning the evolution of the nanocrystalline $LiNbO_3$ phase in the glass system $(100-x)LiBO_2$-xNb_2O_5 ($5 \leqslant x \leqslant 20$, in molar ratio) and its structural, thermal and nonlinear optical properties are elucidated.

Transparent glasses of various compositions in the above system were fabricated via the conventional melt quenching technique. The platinum crucible containing the above mixture covered with a lid was placed in a melt-quenching programmable furnace (Lenton), the temperature was raised to 1373 K (the heating rate used was 5 K/min), and maintained at this temperature for 1 h. Subsequently, the melt was poured onto a preheated (400 K) stainless steel plate and quickly pressed by another plate to obtain 1–1.5 mm thick glass plates. All these samples were heated at 573 K for 6 h (the heating and cooling rates were 50 K/h), well below the glass transition temperature to anneal out the thermal stresses that are likely to be associated with them.

The glassy state of the as-quenched samples was established by subjecting the powders (weighing ≈20 mg) to differential thermal analyses (DTA) (STA 1500, Polymer Laboratory) in the 300–1100 K temperature range. A uniform heating rate of 10 K/min was employed for this purpose. The average values of the glass transition temperature (T_g) and the temperature of onset of crystallization (T_{cr}) were evaluated based on the DTA data collected on more than three samples of each composition. X-ray powder diffraction (XRD) (Scintag) studies were performed at room temperature on the as-quenched and heat-treated samples to confirm their amorphous and crystalline nature respectively. Transmission electron microscopy (TEM) and selected area electron diffraction (SAED) studies were conducted using a JEOL JEM 200CX microscope.

The optical transmission spectra of these samples were recorded at 300 K in the wavelength range 190–3000 nm, using a CARY 5000 varian UV-VIS-NIR spectrophotometer. The second harmonic (532 nm) intensity of the glasses comprising nanocrystallites was measured at 300 K using the Maker-Fringe method. The details of the SHG setup that was used for the measurement were reported elsewhere.[13] The source is a Q-switched Nd:YAG laser operating at 1064 nm wavelength. The Raman spectra were recorded at room temperature in the backscattering geometry using the labram confocal Raman microscope (Dilor) (typical resolution of 4 cm^{-1}).

The DTA traces that were obtained for the as-quenched glass pieces corresponding to the representative compositions $x=5$, 10, 15, and 20 are shown in Figs. 1(a)–1(d). A major exothermic event along with less intense ones are observed for all the as-quenched samples. The samples heat-treated at the onset temperatures of the major exothermic peaks did not exhibit these peaks on subsequent DTA studies, confirming these to be crystallization temperatures. These exotherms indeed shift towards lower temperatures with in-

a)Author to whom correspondence should be addressed; electronic mail: kbrvarma@mrc.iisc.ernet.in

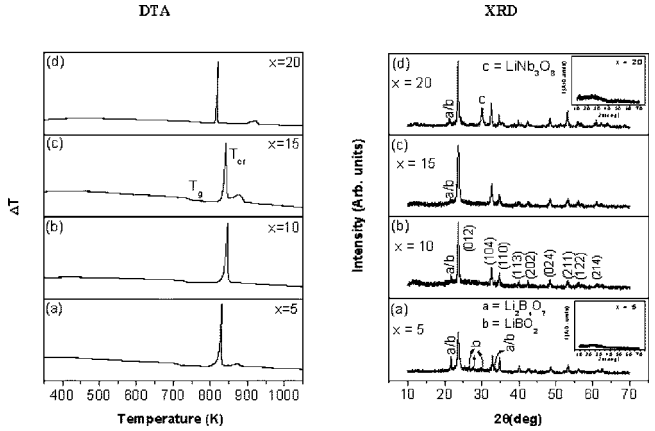

FIG. 1. Differential thermograms for the as-quenched samples and XRD patterns for the sample heat-treated at 773 K/3 h of various compositions.

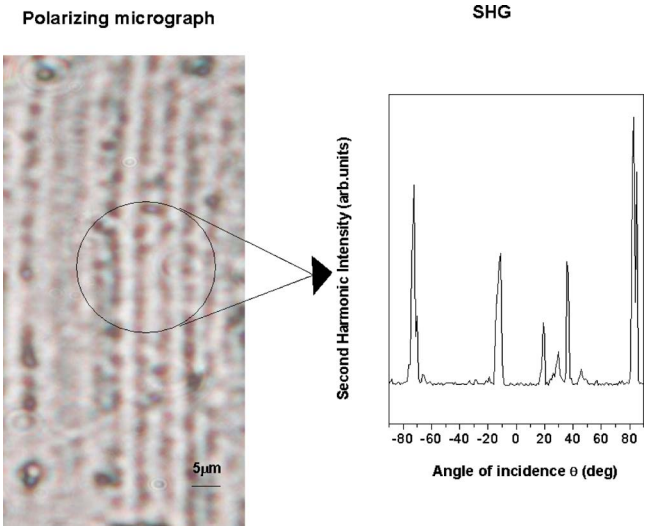

FIG. 2. Polarizing micrograph for the laser irradiated sample of the composition $x=10$ and second-harmonic intensity as a function of the incident angle of the laser (1064 nm) for the as-quenched sample of the composition $x=10$.

crease in x. The x-ray powder diffraction (XRD) patterns of the as-quenched glasses corresponding to the composition $(100-x)LiBO_2$-xNb_2O_5 (where $x=5$ and 20) confirm their amorphous nature [insets in Fig. 1(a) and 1(d)]. The XRD patterns recorded for the samples ($x=5$, 10, 15, and 20) heat-treated in the vicinity of first exotherm (≅773 K) are shown in Figs. 1(a)–1(d). The d-spacings that are obtained based on these patterns are in good agreement with those reported in the literature for a polycrystalline $LiNbO_3$ phase prepared by the conventional solid state reaction route.[14] The lattice parameters ($a=b=5.149$ and $c=13.846$ Å) computed based on the present data are in close agreement with those ($a=b=5.1494$ and $c=13.862$ Å) reported in the literature for $LiNbO_3$. XRD recorded for the composition $x=20$ [Fig. 1(d)], shows Bragg reflections at $2\theta=30.15$ in addition to the $LiNbO_3$ reflections which corresponds to the centrosymmetric $LiNb_3O_8$ phase.[15] It is also observed that the intensity of the peaks corresponding to the $LiNb_3O_8$ phase formation increases with increase in the Nb_2O_5 composition ($x \geqslant 20$). For lower values of x ($x=5$), apart from the presence of the major $LiNbO_3$ phase, we did observe low intense peaks ($2\theta=21.75$ and 25.39) [Fig. 1(a)] corresponding to either $LiBO_2$ or $Li_2B_4O_7$ phases. It implies that, apart from major $LiNbO_3$ phase, the matrix has crystalline $LiBO_2$ or $Li_2B_4O_7$ as a minor impurity phase.

Transmission electron microscopic along with the selected area electron diffraction studies carried out on the as-quenched and heat-treated (773 K) samples of the representative composition $x=10$ confirm its amorphous nature. The presence of local ordered regions (≅3 nm) were found to exist. The sample that was subjected to two-stage heating (733 K/6 h and 773 K/3 h) reveals the presence of spherical crystallites in the glass matrix. The average crystallite size was around 25 nm. The d-spacings obtained based on the selected area electron diffraction (SAED) pattern are 3.70, 2.70, 2.34, 2.21, 1.89, 1.76, 1.69, and 1.51 Å. These are in close agreement with those reported for the $LiNbO_3$ phase. The crystallite size in the samples directly heated to 773 K/3 h (single stage) is found to be ≅100 nm.

The optical transmission spectra recorded at room temperature for the as-quenched glass sample of the representative composition $x=10$ in the wavelength range 190–3000 nm is shown as an inset in Fig. 3. The sample has wide transmission window starting from near infrared to about 350 nm. The SHG (532 nm) intensity collected as a function of the incident angle for the representative composition $x=10$ is shown in Fig. 2. The intense second harmonic signal was found (pulse energy levels of 0.75 to 2.5 mJ) to undergo an optical diffraction. The intensity of which has a strong dependence on the angle of rotation of the sample. In order to have an insight into this phenomenon, subsequent to the SHG experiments, the samples were examined under polarizing microscope (Fig. 2). The surface of the sample interestingly revealed the presence of self-organized parallel damage patterns owing to the interaction of the laser field with the sample. Indeed similar grating-like damage patterns

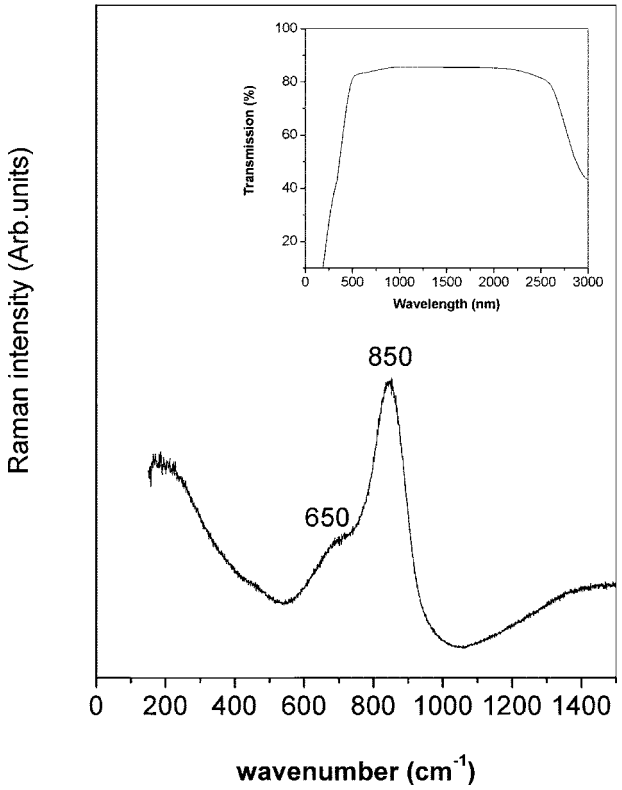

FIG. 3. Micro-Raman spectra at room temperature for the laser irradiated sample of the composition $x=10$. Optical transmission is shown as the inset.

were reported in intrinsic and extrinsic semiconductors[16–22], metals,[23–26] and dielectrics[27] using cw or picosecond laser sources between 0.53 and 10.6 μm. The occurrence of these patterns were interpreted in terms of properties of the laser beam,[16] frozen surface acoustic waves,[19] and plasmon condensation.[25,28]

In the present system it should be noted that, to begin with (i.e., before irradiating with the laser beam) the as-quenched glasses of the all the compositions contained randomly distributed nanocrystallites. These nanocrystallites ($\approx$2 to 3 nm) act as light scattering centers. When the laser beam propagates with a component velocity along the surface, it interacts with the crystallites especially on the surface of the sample and gets scattered. The interference between the scattered and incident radiation that occurs along the axis of the scatterers lead to the formation of the interference fringes (i.e., reflected as the striking diffraction patterns (Fig. 2) observed only at certain angles which correspond to the axis of these scatterers, when the sample is tilted as a function of the incident angle). Hence, the damage fringes which are produced parallel to the scatterers in the present study has been attributed to the interference of the incident beam with the surface-scattered waves originating from the scattering centers.[29]

The parallel damage fringes are separated by a distance (d) equals to $\lambda/1+\sin\theta$, where λ is the wavelength of the incident light and θ is the angle of incidence measured from the surface normal. The interfringe spacings that are found experimentally from polarizing micrograph (Fig. 2) are in good agreement with those predicted by the above formula. Closer examination of the surface revealed that these fringes are actually consisting of a row of equally spaced fine crystallites of submicrometer (0.4 to 0.8 μm) size. The increase in crystallite size from nano to micrometer level in the irradiated samples is ascribed to the localized heating effects created by the intense input laser radiation. The rise in temperature is estimated to be about 740 K at a distance of about 25 μm from the surface of the sample by using the formula[30]

$$\Delta T = \frac{E(1-R)\alpha}{C}, \tag{1}$$

where E is the laser fluence, C the volume specific heat, R is the reflection coefficient, and α the absorption coefficient. The strong electric field vector (estimated to be 10^{12} V/cm) that is associated with the incident laser beam assisted by rise in temperature would result in aligning the crystallites. The formation of self-organized patterns along the parallel damage fringes would diffract light as the crystallite sizes are of same order as that of the wavelength of the SHG light. In order to ascertain the composition of the row of crystallites, micro-Raman spectra were recorded on these lines in the 150–1500 cm^{-1} range (Fig. 3). The peaks at 650 and 850 cm^{-1} which are close to those reported for $LiNbO_3$[31] correspond to a vibrational mode of Nb–O in NbO_6 octahedra.

In conclusion, evolution of $LiNbO_3$ has been demonstrated in a reactive glass system $LiBO_2$–Nb_2O_5. Self-organized crystalline structure formation has been encoded in the present system by infrared (IR) pulsed laser beam in the process of studying its nonlinear optical properties. The diffraction of second harmonic signal is attributed to the presence of well-aligned submicrometer sized $LiNbO_3$ crystallites.

The authors thank the Department of Science and Technology (DST), Government of India, for financial grant. One of the authors (K.B.R.V.) thanks the French Embassy, New Delhi for sponsoring his visit to ICMCB, Bordeaux, France.

[1] N. F. Borrelli, J. Appl. Phys. **38**, 4243 (1967).
[2] M. M. Layton and J. W. Smith, J. Am. Ceram. Soc. **58**, 435 (1975).
[3] A. M. Glass, M. E. Lines, K. Nassau, and J. W. Shiever, Appl. Phys. Lett. **31**, 249 (1977).
[4] T. Kokubo and M. Tashiro, Bull. Inst. Chem. Res., Kyoto Univ. **54**, 582 (1976).
[5] S. Ito, T. Kokubo, and M. Tashiro, J. Mater. Sci. **13**, 930 (1978).
[6] G. Senthil Murugan, K. B. R. Varma, Y. Takahashi, and T. Komatsu, Appl. Phys. Lett. **78**, 4019 (2001).
[7] M. Imaoka and T. Yamazaki, J. Ceram. Soc. Jpn. **76**, 160 (1968).
[8] T. Komatsu, H. Tawarayama, H. Mohri, and K. Matusita, J. Non-Cryst. Solids **135**, 105 (1991).
[9] M. V. Shankar and K. B. R. Varma, J. Non-Cryst. Solids **243**, 192 (1999).
[10] H. G. Kim, T. Komatsu, R. Sato, and K. Matusita, J. Non-Cryst. Solids **162**, 201 (1993).
[11] N. Syam Prasad and K. B. R. Varma, J. Am. Ceram. Soc. **88**, 357 (2005).
[12] M. M. Abouelleil and F. J. Leonberger, J. Am. Ceram. Soc. **72**, 1311 (1989).
[13] V. Rodriguez and Claude Sourisseau, J. Opt. Soc. Am. B **19**, 2650 (2002).
[14] JCPDS-International center for diffraction data, 20–0631.
[15] JCPDS- International center for diffraction data, 36-0307.
[16] M. Birnbaum, J. Appl. Phys. **36**, 3688 (1965).
[17] D. C. Emmony, R. P. Howson, and L. J. Willis, Appl. Phys. Lett. **23**, 598 (1973).
[18] H. J. Leamy, G. A. Rozgonyi, T. T. Sheng, and G. K. Celler, Appl. Phys. Lett. **32**, 535 (1978).
[19] G. N. Maracas, G. L. Harris, C. A. Lee, and R. A. McFarlane, Appl. Phys. Lett. **33**, 453 (1978).
[20] M. Oron and G. Sorensen, Appl. Phys. Lett. **35**, 782 (1979).
[21] J. F. Young, J. E. Sipe, M. I. Gallant, J. S. Preston, and H. M. Van Driel, in *Laser and Electron Beam Interactions with Solids*, edited by B. R. Appleton and G. K. Celler (North-Holland, Amsterdam, 1982), p. 233.
[22] P. M. Fauchet and A. E. Siegman, Appl. Phys. Lett. **40**, 824 (1981).
[23] T. E. Zavecz and M. A. Saifi, Appl. Phys. Lett. **26**, 165 (1975).
[24] J. C. Koo and R. E. Slusher, Appl. Phys. Lett. **28**, 614 (1976).
[25] N. R. Isenor, Appl. Phys. Lett. **31**, 148 (1977).
[26] A. K. Jain, V. N. Kulkarni, D. K. Sood, and J. S. Uppal, J. Appl. Phys. **52**, 4882 (1981).
[27] P. A. Temple and M. J. Soileau, IEEE J. Quantum Electron. **QE-17**, 2067 (1981).
[28] J. A. Van Veachten, Solid State Commun. **39**, 1285 (1981).
[29] D. C. Emmony, R. P. Howson, and L. J. Willis, Appl. Phys. Lett. **23**, 598 (1973).
[30] P. E. Dyer, R. J. Farley, R. Giedl, and D. M. Karnakis, Appl. Surf. Sci. **96**, 537 (1996).
[31] E. B. De Araujo, J. A. C. De Paiva, J. A. Freitas, Jr., and A. S. B. Sombra, J. Phys. Chem. Solids **59**, 689 (1998).